Mechanisms of air-sea CO_2 flux variability in the equatorial Pacific and the North Atlantic

Galen A. McKinley,[1,2] Michael J. Follows, and John Marshall

Department of Earth, Atmospheric and Planetary Sciences, Massachusetts Institute of Technology, Cambridge, Massachusetts, USA

Received 24 October 2003; revised 12 March 2004; accepted 2 April 2004; published 28 May 2004.

[1] A global ocean general circulation model is used to estimate the magnitude of interannual variability in air-sea fluxes of CO_2 and O_2 from 1980–1998 and to examine the controlling mechanisms. The global variability in the air-sea flux of carbon ($\pm 0.5 \times 10^{15}$ grams Carbon yr^{-1} (PgC yr^{-1})) is forced by changes of ΔpCO_2 and wind speeds related to the El Niño/Southern Oscillation (ENSO) cycle in the equatorial Pacific. In contrast the air-sea O_2 flux is controlled by two regions: the equatorial Pacific and North Atlantic. The model captures much of the interannual variability of the CO_2 flux observed at Bermuda, with some correlation with the North Atlantic Oscillation (NAO) index. However, basin-scale air-sea CO_2 flux anomalies are not correlated with the NAO due to a rapid neutralization of entrained DIC anomalies by biological uptake and export production in the subpolar gyre. CO_2 flux variability estimates from our ocean model and the mean atmospheric inversion results of *Bousquet et al.* [2000] are in broad agreement in the equatorial Pacific, but not in the North Atlantic. This model suggests that the projection of air-sea flux anomalies onto the large-scale, mean air-sea flux pattern in atmospheric inversions may lead to an overestimate of the flux variability in the extra-tropics where the patterns of variability do not correspond to those of the mean flux. *INDEX TERMS:* 4215 Oceanography: General: Climate and interannual variability (3309); 4255 Oceanography: General: Numerical modeling; 4805 Oceanography: Biological and Chemical: Biogeochemical cycles (1615); 4806 Oceanography: Biological and Chemical: Carbon cycling; *KEYWORDS:* air-sea exchange, carbon flux, ocean modeling

Citation: McKinley, G. A., M. J. Follows, and J. Marshall (2004), Mechanisms of air-sea CO_2 flux variability in the equatorial Pacific and the North Atlantic, *Global Biogeochem. Cycles*, *18*, GB2011, doi:10.1029/2003GB002179.

1. Introduction

[2] The increase of atmospheric CO_2 is modulated by the natural carbon cycle such that only about half of the CO_2 emitted due to anthropogenic fossil fuel combustion, cement production, and land use change resides in the atmosphere. The remaining CO_2 is taken up by the ocean due to the solubility of CO_2 in seawater and into the terrestrial biosphere due to a net increase in biomass. The enormous complexity of the terrestrial and oceanic biogeochemical systems involved in these CO_2 sinks makes them difficult to understand and quantify. Independent estimates of sink magnitudes and their geographical distributions, based on inversions of atmospheric data, differ significantly and have large error bars [*Gurney et al.*, 2002; *Francey et al.*, 2001; *Manning*, 2001; *Rayner et al.*, 1999a; *Keeling et al.*, 1996; *Bender et al.*, 1996; P. Peylin et al., Interannual CO_2 fluxes as deduced by inverse modeling of atmospheric CO_2 and by models of the ocean and the land carbon cycle, submitted to *Global Biogeochemical Cycles*, 2004 (hereinafter referred to as Peylin et al., submitted manuscript, 2004)]. Furthermore, observations indicate that the growth rate of atmospheric CO_2 varies on interannual timescales significantly more than do CO_2 emissions [*Conway et al.*, 1994]. The substantial temporal variability in CO_2 sinks indicated by these observations is also poorly understood. Interannual variability of CO_2 sinks may hold valuable clues to the mechanisms driving these sinks.

[3] In a previous study with a global circulation and carbon cycle model, *LeQuéré et al.* [2000] find that the modeled estimate of the interannual variability in the global air-sea carbon flux is small relative to the variability implied by atmospheric inversions. *Obata and Kitamura* [2003] report similar results based on a different ocean model. In these models, the global variability is controlled by the equatorial Pacific. However, the circulation model used by *LeQuéré et al.* [2000] was a ''robust diagnostic'' configuration in which temperature and salinity were strongly restored to climatology beneath the surface mixed layer. This may have reduced extra-tropical variability by damping changes in mode water formation rates, for example. In

[1] Now at Department of Atmospheric and Oceanic Sciences, University of Wisconsin-Madison, Madison, Wisconsin, USA.

[2] Now at Program in Atmospheric and Oceanic Sciences, Princeton University, Princeton, New Jersey, USA.

0886-6236/04/2003GB002179

addition, our previous work with a regional North Atlantic oxygen cycle model [*McKinley et al.*, 2000], and a more detailed analysis of the oxygen fluxes in the global model described here [*McKinley et al.*, 2003], show a significant role for the North Atlantic in modulating the air-sea oxygen flux on annual timescales. Could this region also be significant in terms of carbon fluxes? In a recent study, *Gruber et al.* [2002] extrapolate the air-sea carbon flux variability at Bermuda over the North Atlantic basin and suggest that this region should play a significant role globally. The Atlantic is certainly important to the net global CO_2 uptake into the ocean, estimated by *Takahashi et al.* [2002] to be 40% of the global anthropogenic total, despite only occupying 24% of the area of the global ocean.

[4] In this study, we seek to understand and quantify mechanisms of interannual variability of the ocean CO_2 sink using a biogeochemical ocean model driven by state of the art ocean circulation state estimates which do not use the robust diagnostic formulation. We focus on the mechanisms of variability in the equatorial Pacific, which dominates the global flux variability of CO_2. We examine in detail the fluxes and mechanisms in the North Atlantic in the light of our previous oxygen studies [*McKinley et al.*, 2000, 2003] and those of *Gruber et al.* [2002] and *Bousquet et al.* [2000], focusing on the importance of the Atlantic to global variability. We investigate the potential implications of the spatial structure of the CO_2 flux variability in our model on atmospheric inversion estimates of the ocean CO_2 sink variability.

[5] This paper is organized as follows. In section 2, we describe the ocean biogeochemical model. In section 3, we describe the global scale interannual variability of the model and the relative contributions from each of the ocean basins. In section 4, we focus on the mechanisms at play in the equatorial Pacific and North Atlantic. In section 5, we summarize and conclude.

2. Biogeochemical Ocean Model

[6] The offline biogeochemical model is based upon the MIT Ocean General Circulation Model [*Marshall et al.*, 1997a, 1997b]. An offline model is a tracer-only model for which all mean and time-varying physical properties (advection, temperature, etc.) are pre-computed, archived fields. Physical model results are from a simulation made at the Jet Propulsion Laboratory, covering the period 1980–1998 [*Lee et al.*, 2002]. Horizontal resolution is 1° in longitude, 1° in latitude at high latitudes and telescoping to 0.3° in the tropics. The circulation model has 47 vertical levels, with 10-m resolution between the surface and 150 m. The Gent-McWilliams [*Gent and McWilliams*, 1990] eddy parameterization and the KPP boundary layer mixing scheme [*Large et al.*, 1994] are used to represent subgridscale processes. The general circulation model is forced with 12-hourly reanalyzed wind stress, heat, and freshwater fluxes. Sea surface temperature (SST) is relaxed to the National Centers for Environmental Prediction (NCEP) [*Kalnay et al.*, 1996] reanalysis with a timescale dependent on the deviation from the reanalysis. Similarly, sea surface salinity (SSS) is relaxed to the climatology of *Conkright et al.* [1998]. Ten-day average advective fields, Gent-McWilliams tensors and background diffusion, KPP mixing coefficients, and temperature and salinity fields are used to drive the offline model.

[7] In Figure 1, model mixed layer depths are compared to observations at the Bermuda Atlantic Time series Station (BATS) and at the Hawaii Ocean Time series (HOT) for the period 1989–1998 [*Bates*, 2001; *Karl and Lukas*, 1996]. At BATS, the modeled mixed layer depth is consistent with the observed seasonal cycle, though it is somewhat too deep in winter. The model captures the magnitude of mixed layer depth variability as well as a good portion of the detailed features. While the overestimate of winter deep mixing and some lack of correspondence of the variability could significantly impact productivity and CO_2 fluxes [*Bates*, 2001], we show in section 3.2 that CO_2 flux variability is actually quite well captured at BATS. At HOT, the seasonal cycle of the mixed layer is well captured by the model. In both the observations and the model, the seasonal and interannual variability at HOT is much smaller than at BATS. The model underestimates the interannual variability at HOT.

[8] To evaluate the model's representation of observed physical variability on the larger scale, we compare zonally averaged model SST variance to the *Reynolds and Smith* [1994] climatology in Figure 2. The model captures the magnitude of the SST variance together with all the major observed features. This is particularly significant for the consideration of air-sea CO_2 fluxes because SST is a major driver of the pCO_2 seasonal cycle across much of the global oceans [*Takahashi et al.*, 2002], and therefore is likely to be important to its interannual variability. The model's overrepresentation of the SST variance in the North Atlantic between 40°N and 60°N is because the modeled Gulf Stream is too broad.

[9] Analysis of the physical model indicates that it captures approximately 35% of the TOPEX/Poseidon observed sea surface height (SSH) variability [*McKinley*, 2002] when both the satellite data and model results are averaged to 2° × 2° or coarser resolution. This degree of SSH variance representation is similar to that found by *Stammer et al.* [1996] in a 1/4° ocean model, indicating that the model does quite well given its resolution.

[10] The underrepresentation of SSH and mixed layer depth variability is due to the lack of explicitly resolved mesoscale eddies, the boundary conditions with which the model is forced, and the imperfect parameterizations used to represent sub-gridscale processes. This underestimate of the level of physical variability suggests that air-sea gas flux variability estimates derived from the model are likely to be lower bound estimates.

[11] The prognostic variables of the biogeochemical model are dissolved inorganic carbon, *DIC*, total dissolved phosphorus, *P* and dissolved oxygen, O_2. The governing equation for DIC is

$$\frac{\partial DIC}{\partial t} = -\nabla\cdot(\mathbf{u}DIC) + \nabla\cdot(K\nabla DIC) + R_{C:P}\cdot S_b + FW_{DIC} + E_{DIC}, \quad (1)$$

where **u** is the transformed Eulerian mean velocity (incorporating advective transport by both the mean flow

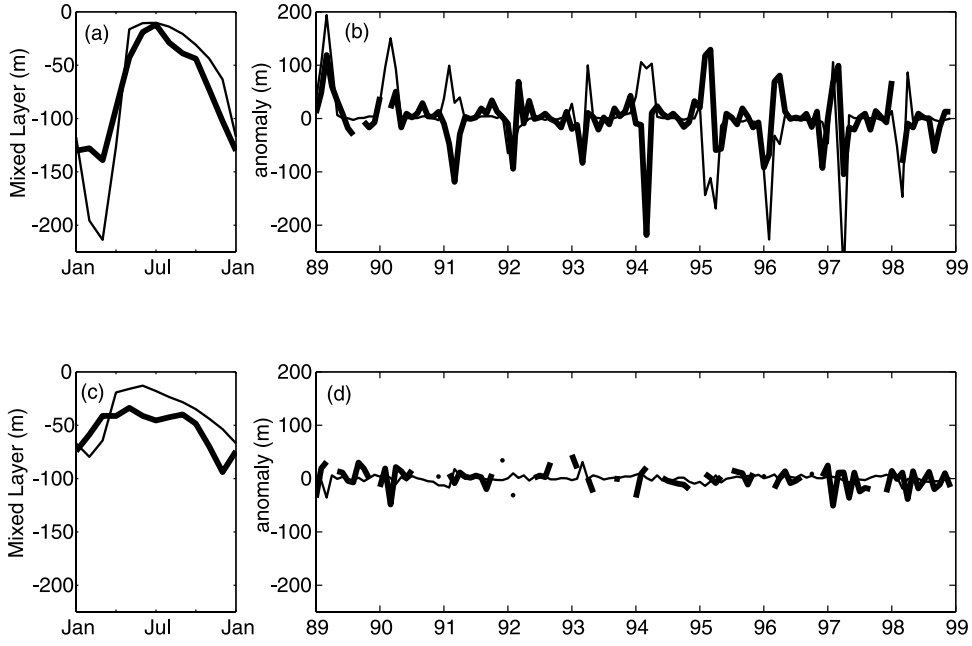

Figure 1. Model (thin solid line) and observed (bold solid line) mixed layer depths 1989–1998: (a) mean cycle at BATS, (b) variability at BATS, (c) mean cycle at HOT, and (d) variability at HOT. A mixed layer depth criteria of $\Delta\rho = 0.125$ kg m^{-3} is applied to both the monthly data and the model results [*Monterey and Levitus*, 1997].

and eddies) and $\nabla \cdot (K\nabla DIC)$ is a tensorial representation of the sub-gridscale mixing schemes [*Gent and McWilliams*, 1990; *Large et al.*, 1994] of the physical model. A third-order upwind, flux-corrected advection scheme is used in the offline tracer model [*Dutkiewicz et al.*, 2001]. As described in detail below, S_b represents both the loss of P due to the biological formation of sinking particles and a source of P from remineralization. Here we assume that biological changes to DIC respond in proportion to changes in P based on the Redfield ratio, $R_{C:P} = 117{:}1$ [*Anderson and Sarmiento*, 1994]. FW_{DIC} represents the dilution (or virtual fluxes) of tracers due to surface freshwater fluxes, and E_{DIC} denotes air-sea gas exchange. The oxygen model, with prognostic equation similar to that for DIC above, is described in more detail by *McKinley et al.* [2003].

[12] We apply an idealized parameterization of export production limited by light and phosphate availability. All other controlling factors are represented by a regionally adjustable maximum export rate, $\alpha(x, y)$. For each layer in the model's euphotic zone (0–140 m), the export of nutrients is determined by

$$B(z) = -\alpha(x,y) \cdot \left(\frac{I(y,z,t)}{I(y,z,t) + I_o}\right) \cdot \left(\frac{P(x,y,z,t)}{P(x,y,z,t) + P_o}\right). \quad (2)$$

The value of the maximum export rate, α, encapsulates all the processes leading to export which are not represented by the explicit phosphate and light limitation. These unresolved processes might include, for example, regional variations in grazing efficiency, recycling, or iron limitation. All temporal variation is assumed due to phosphate and light variability. $I(y, z, t)$ is the flux of photosynthetically active radiation (PAR) at the surface and with depth in the ocean which varies with both season and latitude. The half-saturation constant for light (I_o) is 30 W m^{-2} in PAR, and for phosphate (P_o) is 0.01 μmol kg^{-1}. The sinking particle flux (F(z)) is parameterized as a function of depth following

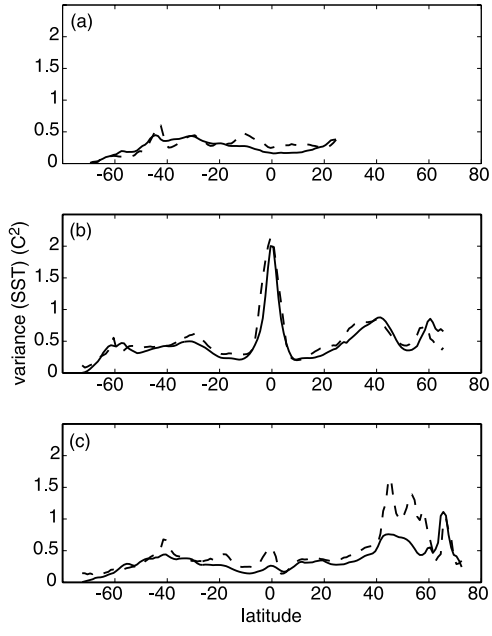

Figure 2. Model (dashed line) and observed (solid line) zonally averaged SST variance for (a) Indian Ocean 60°E–90°E, (b) Pacific Ocean 180°E–150°E, and (c) Atlantic Ocean 50°W–10°W. Data and model results are averaged over 2° × 2° boxes prior to the variance calculation.

Table 1. Ocean Regions, Boundaries, Maximum Export Rate (α), and Export Timescale[a]

Region	Boundaries	α, 10^{-8} μmol kg^{-1} s^{-1}	τ, Years
Southern Ocean	80°S–55°S	4.6	1.3
Subantarctic	55°S–35°S	4.3	0.73
South Indian	35°S–15°S, 22°E–140°E	0.25	3.2
North Indian	15°S–26°N, 38°E–108°E	1.2	1.8
Subtropical South Pacific	35°S–15°S, 145°E–295°E	0.76	1.2
Subtropical South Atlantic	35°S–15°S, 295°E–22°E	1.4	0.86
Eastern equatorial Pacific	15°S–15°N, 200°E–283°E	1.8	1.4
Western equatorial Pacific	15°S–15°N, 109°E–200°E	2.3	0.65
Equatorial Atlantic	15°S–15°N, 284°E–25°E	1.1	1.6
Subtropical North Pacific	15°N–44°N, 105°E–267°E	2.2	0.54
Subtropical North Atlantic	15°N–44°N, 267°E–354°E	2.6	0.23
Subpolar North Pacific	45°N–79°N, 115°E–240°E	2.4	2.1
Subpolar North Atlantic	45°N–79°N, 266°E–20°E	77.2	0.03
Mediterranean	30°N–44°N, 355°E–38°E	10.3	0.04

[a]Export timescale τ is calculated from α and the mean phosphate over the specified region [*Conkright et al.*, 1998].

[*Dutkiewicz et al.*, 2001]. Within the euphotic zone, $S_b = B(z) + F(z)$ and below, $S_b = F(z)$.

[13] Similar particle export parameterizations have been used with constant parameter values in the North Atlantic [*McKinley et al.*, 2000; *Williams and Follows*, 1998]. When combined with various representations of light limitation, the resulting fallout timescales are of order a week in the summer to many years in the high latitude winter. These models have been able to capture the major features and annual cycles of nutrients in the North Atlantic. *Maier-Reimer* [1993] has used such a model with a constant export factor to calculate production in the HAMMOC3 global ocean model. He finds reasonable agreement with surface nutrient observations in most of the ocean, but significantly overestimates new production and underestimates pCO_2 in the eastern equatorial Pacific.

[14] In order to avoid these effects, we build on the simplified prognostic form for export production presented in equation (2) to derive a spatially inhomogeneous α for use in this model. Following the example of *Marshall and Molteni* [1993], who determine spatially varying potential vorticity flux forcings for a quasigeostrophic model of the atmosphere, we solve for an $\alpha(x, y)$ that, given model flow fields, will produce an annual mean phosphorous distribution consistent with climatological observations [*McKinley*, 2002]. The result is a spatially varying $\alpha(x, y)$ into which all unknowns of the biological system are incorporated. As this method requires a consistency of the model circulation and climatological nutrient fields, α is adjusted only on the large scale, over 14 basin-scale regions, where such consistency is possible. The export timescales ($\tau(x, y)$) of the solution for $\alpha(x, y)$ are broadly consistent with known controls on export in the global ocean (Table 1). The shortest timescales are found in the northern subtropical gyres and in the subpolar North Atlantic. In contrast, long export timescales in the Southern Ocean, the eastern Equatorial Pacific, and the subpolar North Pacific are consistent with the High Nutrient/Low Chlorophyll regions where iron limitation is the likely control [e.g., *Martin et al.*, 1994]. In short, the substantial heterogeneity of α adjusts the broad regional patterns of export production to bring the modeled nutrient field into consistency with the observed climatology. The resulting pattern of α is consistent with current understanding of regional biogeochemistry.

[15] Air-sea gas exchange is parameterized following *Wanninkhof* [1992]. The proportionality constant (a) from *Wanninkhof* [1992] equation (3) is determined based on the frequency distribution of our 12-hour winds speeds (Comprehensive Ocean-Atmosphere Data Set (COADS) [*da Silva et al.*, 1994] mean with NCEP variability, 1980–1998). We find $a = 0.39$. The method of J. Boutin and J. Etcheto (Climatology of K deduced from the satellite wind speeds, 1995, available at http://www.ipsl.jussieu.fr/OCMIP/phase1/distrib/README.satdat) is used to determine a 10-day average squared wind speed product for use in the model that fully accounts for 12-hourly wind speed variability ($\bar{u}_{10}^2 + \sigma_{u_{10}}^2$, where u_{10} is the wind speed at 10 m). Since here we are primarily interested in the response of air-sea gas exchange to changing physical forcing, a constant atmospheric pCO_2 of 354 ppm is applied; a mean value observed in 1990 at Mauna Loa [*Keeling and Whorf*, 2000]. Likewise, a constant atmospheric pO_2 of 20.946 pph is applied. Seasonal variation of atmospheric pCO_2 is not considered and so there is potential for flux bias, particularly at high latitudes where seasonal variability can be as large as 10 ppm. Surface ocean pCO_2 is determined from the local DIC concentration, alkalinity, temperature, salinity, and borate concentration as given by *Follows et al.* [1996]. Alkalinity is assumed to be a linear function of salinity based on GEOSECS data after *Campbell* [1983]. Borate equilibrium is determined following *Takahashi et al.* [1981], with a globally constant dissolved inorganic boron concentration of 409 μmol/kg.

[16] Net freshwater fluxes to the surface layer are used to drive a dilution, or virtual flux, of tracers. Fluxes are a combination of the model forcing (COADS mean with NCEP variability) and the virtual fluxes due to sea surface salinity relaxation from the physical model. We apply climatological monthly ice coverage maps as used in the Ocean Carbon-Cycle Model Intercomparison Project (J. Orr et al., Ocean Carbon-Cycle Model Intercomparison Project 2: Abiotic-HOWTO, 2002 (available at http://www.ipsl.jussieu.fr/OCMIP/)) [*Dutay et al.*, 2002]. Both gas exchange and export production are reduced proportional

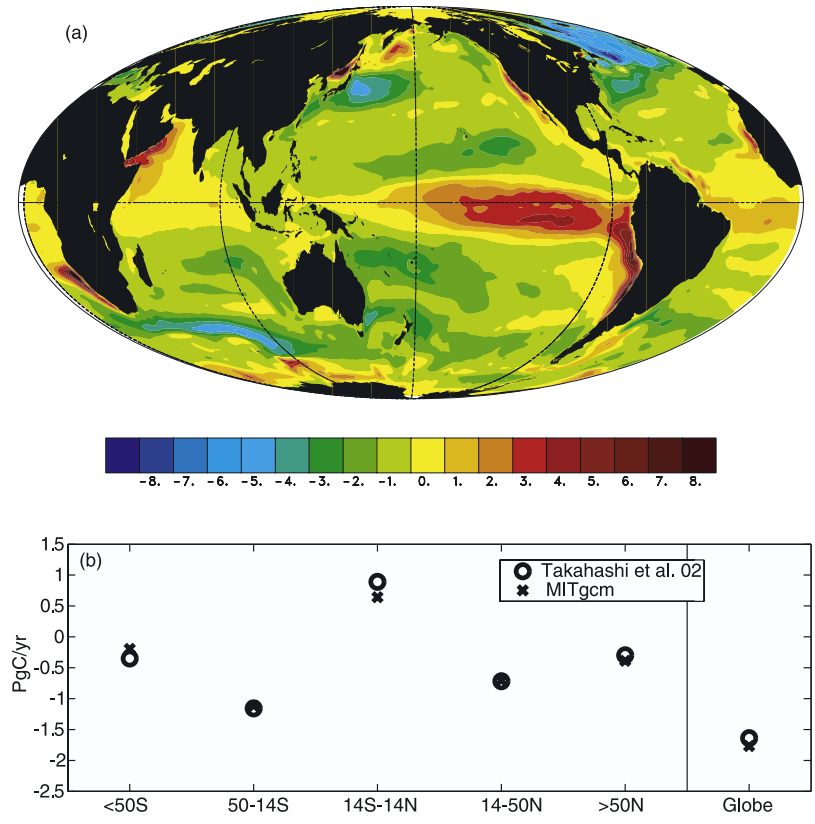

Figure 3. (a) Mean CO_2 flux (mol m^{-2} yr^{-1}), and (b) zonally average comparison to the corrected *Takahashi et al.* [2002] result (http://www.ldeo.columbia.edu/CO2/). Positive fluxes are to the atmosphere.

to the amount of ice cover once the cover is greater than 20%. Nutrients and oxygen distributions are initialized from the climatology of *Conkright et al.* [1998] and DIC from the climatology of *Goyet et al.* [2000].

[17] The offline biogeochemical model is run only in the upper ocean (0–1265 m), and relaxation to the initialization climatologies occurs in the bottom three layers (965–1265 m). The assertion by *LeQuéré et al.* [2003] that this configuration applies to our physical simulation is incorrect: The physical model is run prognostically throughout the ocean. The annual climatology of the 19 years (1980–1998) of model physical fields is used to force the model during a 21-year spinup and then one time through the fields for 1980. The model is then restarted at 1980 and driven through the 19-year, time-varying circulation fields with a 2-hour time step. This spinup "flushes" the initial condition from the ventilated thermocline. While there is some quantitative effect of shifting from climatology to 1980 and then restarting at 1980, analysis shows that this does not change the qualitative result and is insignificant after 2 or 3 years.

3. Modeled Carbon Fluxes and Variability

3.1. Comparison to Mean Flux Estimate of *Takahashi et al.* [2002]

[18] In Figure 3a we depict the 1980–1998 mean air-sea CO_2 flux from the model, with positive fluxes to the atmosphere. The regional patterns compare well to the "climatological" observations of *Takahashi et al.* [2002]. There is net outgassing of CO_2 to the atmosphere across the equatorial Pacific due to wind-driven divergence and upwelling. Other regions of the tropics also act as small net sources of CO_2 to the atmosphere. The subtropics are generally small net CO_2 sinks, and carbon is taken up by the oceans in the high northern latitudes, along the western boundary currents and in the subpolar North Atlantic. In the Southern Ocean, CO_2 enters the model ocean through the cooling of the poleward flowing Agulhas current at the southern tip of Africa. In Figure 3b, zonally averaged mean CO_2 fluxes are compared to the observed estimate. Zonal average mean model fluxes compare very well to the data estimates in all regions and for the globe. Net outgassing occurs in the tropics, and net ingassing occurs in the middle and high latitudes. The global mean CO_2 flux of the model is 1.8 PgC yr^{-1} into the ocean for 1980–1998, quite close to the corrected *Takahashi et al.* [2002] estimate of 1.64 PgC yr^{-1} for 1995 (http://www.ldeo.columbia.edu/CO2/).

[19] It is important to note two caveats that increase the uncertainty of this comparison: (1) A constant atmospheric pCO_2 value has been used in the simulation, and (2) there is a trend in the modeled air-sea flux of CO_2 (see below). Though the atmospheric pCO_2 used in the simulation is not varying in time, it is a mean value for the midpoint of the simulation time period, 1990. The model is also initialized

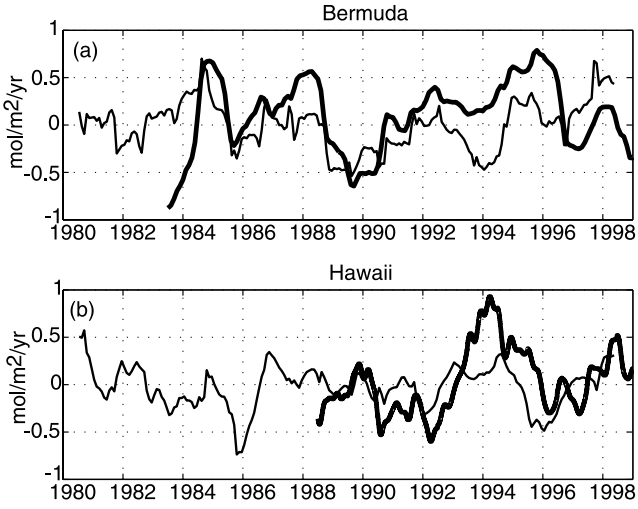

Figure 4. Comparison of model (thin solid line) at (a) Bermuda and (b) Hawaii to observational (bold solid line) estimate of air-sea CO_2 flux variability [*Gruber et al.*, 2002]; (Brix et al., submitted manuscript, 2004). Data and model results are smoothed over 12 months. Model results are an average of a $3° \times 3°$ region centered on the time series locations, so as to be more representative of the region of interest. Positive fluxes are to the ocean.

with a modern-age DIC climatology so that the deep waters coming to the surface have DIC concentrations consistent with the modern ocean. Together, these model choices clearly place the simulation in the anthropogenic age and give us a priori confidence in the validity of a comparison to the observations. The high quality of the comparison shown in Figure 3 also gives a posteriori confidence in assumptions made during model formulation.

[20] The global air-sea flux of CO_2 has a trend of 0.07 PgC yr^{-2} over the course of the 19-year integration, due to the continuing adjustment of the model's deeper waters to surface boundary conditions [*McKinley*, 2002]. Given the resolution, complexity, and computational requirements of the model, as well as our focus on understanding interannual variability, this relatively small drift is acceptable. However, because it is not readily possible to separate this drift from perhaps plausible changes in the ocean tracer budget and air-sea fluxes, we only examine model estimates of interannual variability in air-sea CO_2 fluxes relative to the 19-year trend. The model trend was calculated by a linear fit to the result from which the seasonal cycle has been removed at each point in space, and is removed on a point-by-point basis in the results that follow.

3.2. Global Interannual Variability of Fluxes

[21] Before looking at globally and regionally integrated air-sea flux variability, we consider comparisons of modeled air-sea CO_2 flux variability to observational estimates. At Bermuda (BATS and Station S), we plot the model result and the estimate from observations by *Gruber et al.* [2002] (Figure 4a). The model pleasingly captures both a substantial portion of the magnitude and many features of the observed air-sea flux variability. The RMS variability of the model is 0.27 mol m^{-2} yr^{-1} and that of the observations is 0.35 mol m^{-2} yr^{-1}. In Figure 4b, a similar comparison is shown for the Hawaii station (HOT) using the observational results of H. Brix et al. (Interannual variability of the upper ocean carbon cycle at station ALOHA near Hawaii, submitted to *Global Biogeochemical Cycles*, 2004) (hereinafter referred to as Brix et al., submitted manuscript, 2004). The model has an RMS variability over the observational time period of 0.18 mol m^{-2} yr^{-1}, compared to 0.35 mol m^{-2} yr^{-1} from the data up to 1998. Model RMS variability is 0.22 mol m^{-2} yr^{-1} if the entire 1980–1998 period is considered. Owing to restoration to climatological salinity and model drift, it is not possible for the model to capture the increasing pCO_2 trend of the 1990s at HOT [*Dore et al.*, 2003]. Consistent with previous comparisons of the physical model, these comparisons suggest that the global and regional flux variability estimates from the model are likely to capture many features of the real ocean's variability, but that the magnitude of the variability estimated by the model is likely to be a lower bound. Damped salinity variability and limited physical variability due to the lack of explicit mesoscale eddies and model boundary conditions provide some explanation for the model's underestimate of the observed variations, as was discussed in section 2.

[22] The time series of interannual variability in air-sea CO_2 fluxes is presented in Figure 5a. Interannual variability in the global air-sea CO_2 flux has a maximum amplitude of ±0.5 PgC yr^{-1}, and a RMS of 0.28 PgC yr^{-1}. The model estimate of the interannual variability in the global CO_2 flux is larger than the model of *LeQuéré et al.* [2000]. It is similar in magnitude to that of *LeQuéré et al.* [2003], who add a multicompartment ecosystem to the model of *LeQuéré et al.* [2000]. Concurrent work with CO_2-only [*Bousquet et al.*, 2000] (Figure 12a in section 4.3) and multitracer atmospheric inversions for land and ocean CO_2 sinks [*Francey et al.*, 2001] give smaller estimates of air-sea flux variability of CO_2 than previous efforts [*Rayner et al.*, 1999a] with extremes of a similar magnitude to our model estimate. Thus we see some convergence in terms of flux variability magnitude between models and atmospheric inversions. However, as will be discussed in section 4.3, the spatiotemporal distribution of this variability differs substantially between approaches.

[23] A regional breakdown of the annual anomalies in the CO_2 flux (Figures 5b–5d) illustrates that the global flux variability is largely driven by the equatorial Pacific between 15°S to 15°N (RMS = 0.17 PgC yr^{-1}). The global time series correlates with the equatorial Pacific at r = 0.85. The dominance of the equatorial Pacific to global integrated CO_2 flux variability is consistent with previous modeling studies [*Obata and Kitamura*, 2003; *LeQuéré et al.*, 2000; *Winguth et al.*, 1994] but possibly at odds with independent estimates from atmospheric inverse models which suggest a greater role for the extra-tropics. Consistent with the findings of *Obata and Kitamura* [2003], the Southern Ocean (80°S–30°S) provides the second-largest source of variability (RMS = 0.09 PgC yr^{-1}). In contrast to the suggestion of *Gruber et al.* [2002], the model has a small

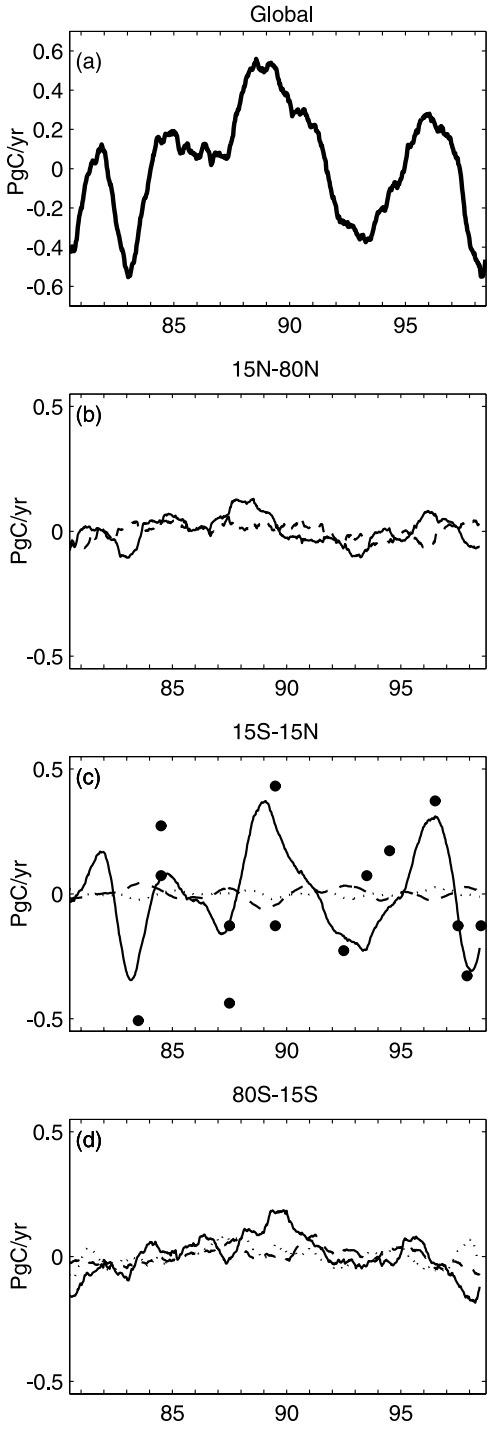

Figure 5. (a) Modeled global interannual variability of air-sea CO_2 fluxes, and regional breakdown for the Pacific (solid line), Atlantic (dashed line), and Indian (dotted line) for (b) 15°N–80°N, (c) 15°S–15°N, and (d) 80°S–15°N. The dots in (c) are the Equatorial Pacific observations complied by *Feely et al.* [1999]. Detrended model anomalies about the 1980–1998 time average are shown. Positive fluxes are to the atmosphere.

CO_2 flux variability in the North Atlantic (RMS = 0.03 PgC yr^{-1}). Yet in a study of this same model [*McKinley et al.*, 2003] we find that the global O_2 flux variability has significant contributions both from the equatorial Pacific and the North Atlantic basin. Hence, in the following sections, we discuss in more detail the physical and biogeochemical variability of this model in the equatorial Pacific and North Atlantic and seek to understand differences in CO_2 and O_2 flux variability.

4. Mechanisms and Fluxes in the Equatorial Pacific and North Atlantic

4.1. Equatorial Pacific

[24] We use empirical orthogonal function (EOF) analysis of model results to determine the most significant pattern of the flux variability and to provide mechanistic clues. The first EOF (EOF1) of the air-sea CO_2 flux variability in the Pacific explains 18% of the variance over the region (Figure 6). In a comparable analysis of just the equatorial Pacific (15°S–15°N), the first EOF explains 50% of the interannual variance, with the same structure across the equator. The EOF1 pattern in Figure 6 clearly reflects the influence of ENSO on the air-sea flux [*Feely et al.*, 2002; *Boutin et al.*, 1999; *Feely et al.*, 1999; *Chavez et al.*, 1999]. The variability pattern is focused in a large region along the equator with its center at 3°S, 135°W; around approximately 10°S on the South American coast; and, to a lesser degree, on the west coast of North America. The first principle component (PC1) correlates with the Southern Oscillation Index (SOI) at r = 0.89 (no lag), indicating a strong influence of ENSO across the subtropical and

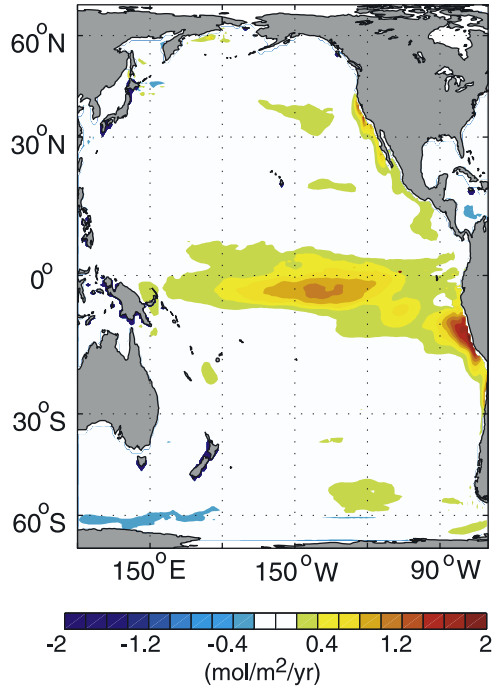

Figure 6. First EOF of the air-sea flux of CO_2 in the Pacific (mol m^{-2} yr^{-1}).

equatorial Pacific. When considering either PC1 or the equatorial flux time series (Figure 5c), we do not find that the ocean CO_2 flux anomaly leads the SOI as was suggested by *Rayner et al.* [1999b]. We find maximum correlations with zero lag for the PC1 or if the flux time series lags the SOI by 1 or 2 months (r = 0.80). Thus, while it is clear that ENSO is the driver of equatorial Pacific CO_2 flux variability, the precise temporal relationship between the SOI and the CO_2 flux remains an open question.

[25] The analysis of *Chavez et al.* [1999] and the models of *LeQuéré et al.* [2000] and *Obata and Kitamura* [2003] find that physically forced surface DIC variability is the major forcing for CO_2 flux variability. We also find that changes in the transport of DIC dominate the model's pCO_2 variability in the equatorial Pacific and this variability in pCO_2 drives, in turn, approximately 70% of the air-sea carbon flux variability. Wind speed variability drives the remaining 30% of the year-to-year flux changes in this region of the model, consistent with analyses of observed data [*Boutin et al.*, 1999; *Feely et al.*, 2002].

[26] In our model, pCO_2 variability is driven through changes in the upwelling rate and the depth of high DIC waters in the eastern equatorial Pacific, and also through longitudinal shifts in the western Pacific warm pool. Under normal conditions, the equatorial Pacific thermocline shallows from west to east and strong upwelling occurs due to Ekman divergence at the equator. This supplies DIC-rich waters to the surface, resulting in the net efflux of CO_2 seen in Figure 3a. In the El Niño phase, the thermocline in the east is depressed by eastward propagating Kelvin waves generated by anomalous westerly wind bursts in the western Pacific [*McPhaden et al.*, 1998]. This downward displacement of the thermocline moves the supply of cold, high pCO_2 water farther from the surface. Slackening of the trade winds leads to reduced Ekman divergence at the equator during El Niño. Also, the western Pacific warm pool shifts to the east to form a warm, low-pCO_2 cap in regions that would normally exhibit upwelling of high pCO_2 waters [*Feely et al.*, 2002]. The combined effect of a depressed thermocline, reduced upwelling, and longitudinal displacement of the warm pool is to significantly alter the amount of high DIC waters exposed to the atmosphere; a positive SST anomaly and negative ΔpCO_2 anomaly form in the equatorial band (Figures 7a and 7b). The negative ΔpCO_2 anomaly is the primary driver of the negative anomaly in air-sea flux of CO_2 (reduced flux of CO_2 to the atmosphere) during El Niño (Figure 7d). In the La Niña phase, the upward slope of the thermocline to the east is enhanced, both bringing high DIC waters closer to the surface and increasing the efficiency of divergence-driven upwelling along the equator, and the region of upwelling extends further to the west [*Feely et al.*, 2002]. This results in a positive CO_2 flux anomaly (Figure 7d).

[27] Air-sea CO_2 flux is modeled as a function of the atmosphere-ocean ΔpCO_2 and the square of the wind speed [*Wanninkhof*, 1992]. Analysis of CO_2 flux variability estimated with the model's interannually varying wind speed forcing and its mean seasonal cycle of ΔpCO_2 indicates that wind variability contributes approximately 30% of the total CO_2 flux variability in the equatorial Pacific. Wind speed variability is not a significant driver of flux variability in other ocean regions. In the equatorial Pacific, ΔpCO_2 and wind speed variability act in concert, and their interannual variability is, in both cases, driven by the ENSO cycle (Figure 7). It is interesting to note that wind speed variability is most important in the central equatorial Pacific, while ΔpCO_2 variability clearly dominates the model CO_2 flux variation toward the east, consistent with the observational studies of *Boutin et al.* [1999] and *Feely et al.* [2002].

[28] *Chavez et al.* [1999] find that during a non-El Niño period in 1995–1996, the CO_2 flux from 10°S to 10°N in the equatorial Pacific had an observed maximum of 6.0 mol m^{-2} yr^{-1}, and that this drops to 0.5 mol m^{-2} yr^{-1} during the El Niño of 1997–1998. Our model gives a maximum flux of 6.5 mol m^{-2} yr^{-1} during the same non-El Niño period and 1.5 mol m^{-2} yr^{-1} during the same El Niño. The modeled flux anomalies in the equatorial Pacific are also in very good agreement with the analysis of *Cosca et al.* [2003], based on in situ data and remote observations. In brief, the modeled interannual variability of the equatorial Pacific air-sea flux is in good agreement with previous data studies and models both in terms of the processes at play and the quantitative estimates.

4.2. North Atlantic

[29] The North Atlantic Oscillation (NAO) and associated phenomena capture a significant fraction of North Atlantic physical variability [*Hurrell*, 1995; *Dickson et al.*, 1996]. In a prior study of the O_2 cycle in this model [*McKinley et al.*, 2003], air-sea flux variability was shown to be strongly influenced by interannual changes in wintertime convective mixing in the region, correlated with the NAO index. It has also been recently postulated that there may be a similar relationship between basin-scale air-sea CO_2 flux in the North Atlantic and the NAO index [*Gruber et al.*, 2002] and that the resulting fluxes could be significant for net global variability. However, the model described here does not support that suggestion. We find (Figure 5) that CO_2 flux variability is rather small in the North Atlantic. EOF1 for the air-sea CO_2 flux in the North Atlantic explains only 11% of the interannual variance (Figure 8a). The pattern of EOF1 is centered in the subpolar region, capturing the regions of deep wintertime convection in the model.

[30] Why does the model not support a significant regional CO_2 flux variability over the North Atlantic? The model captures appropriate aspects of the physical variability. The first EOF of model SST (Figure 8b) illustrates the classic NAO tripole, and the associated time series correlates with the NAO (r = 0.50). Furthermore, the modeled O_2 fluxes [see *McKinley et al.*, 2003] illustrate that there is a biogeochemical response with a significant relationship to the NAO index leading to substantial regional air-sea O_2 flux anomalies. Yet, in contrast, PC1 of the air-sea CO_2 flux EOF1 is uncorrelated with the NAO index. Thus the model indicates a decoupling of the air-sea CO_2 flux variability from the major driver of physical variability in the North Atlantic and a decoupling of the CO_2 and O_2 fluxes.

[31] To understand what controls the CO_2 flux and its relationship to the physical forcing and oxygen, we

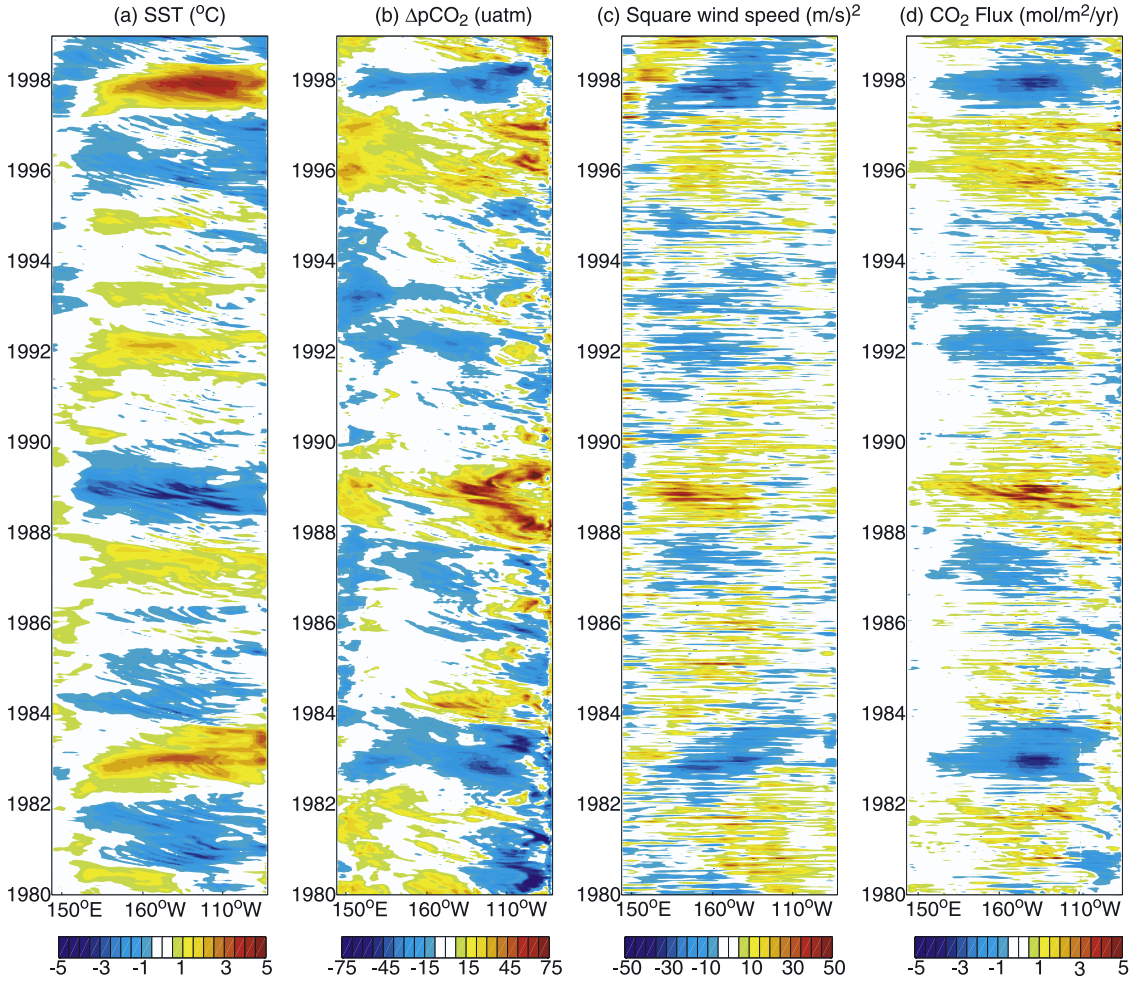

Figure 7. Hovmoller diagrams of the anomalies of (a) model SST (°C), (b) ΔpCO_2 (μatm), (c) squared wind speed model forcing ((m s^{-1})^2), and (d) air-sea CO_2 flux (mol m^{-2} yr^{-1}), all averaged 5°S–5°N in the equatorial Pacific. The strong El Niño events of 1982–1983 and 1997–1998 and the strong La Niña event of 1988–1989 are particularly noticeable. Air-sea flux anomalies are positive to the atmosphere.

diagnose the factors driving the variability in the modeled ocean surface pCO_2. Following *Takahashi et al.* [1993], the effects on pCO_2 of surface DIC concentration, temperature, alkalinity, and salinity may be written in linearized form,

$$\frac{dpCO_2}{dt} = \frac{\delta pCO_2}{\delta DIC}\frac{dDIC}{dt} + \frac{\delta pCO_2}{\delta T}\frac{dT}{dt} + \frac{\delta pCO_2}{\delta ALK}\frac{dALK}{dt} + \frac{\delta pCO_2}{\delta S}\frac{dS}{dt}. \quad (3)$$

[32] In Figures 9a and 9b, the components driving changes in pCO_2 in the model are plotted as a function of location in the subpolar and subtropical gyres, respectively. The analysis of observed data by *Takahashi et al.* [2002] indicates that DIC changes largely drive the pCO_2 seasonal cycle variability in the subpolar North Atlantic, while temperature effects dominate the cycle in the subtropics. Consistently, our model diagnostics indicate that DIC anomalies largely drive the model's subpolar variability in pCO_2. (The total pCO_2 variability and the DIC term correlate at r = 0.78). Temperature anomalies act to slightly damp DIC-driven pCO_2 variability. This is to be expected, since cooler waters are generally richer in DIC with respect to both vertical and horizontal gradients, though we note the effect may be exaggerated since SST variability in this region is overestimated (Figure 2). Also consistent with the findings of *Takahashi et al.* [2002], temperature variability determines pCO_2 variability (r = 0.69) in the model's subtropical Atlantic, while DIC anomalies generally play a smaller role. In general, the underlying drivers of variability in Atlantic pCO_2 are qualitatively consistent with in situ data studies.

[33] The convective supply of nutrients and export production in the modeled North Atlantic show a clear relationship to the NAO index, consistent with observations (primary production) at BATS [*Bates*, 2001] and previous models [*Williams et al.*, 2000]. EOF1 of the North Atlantic

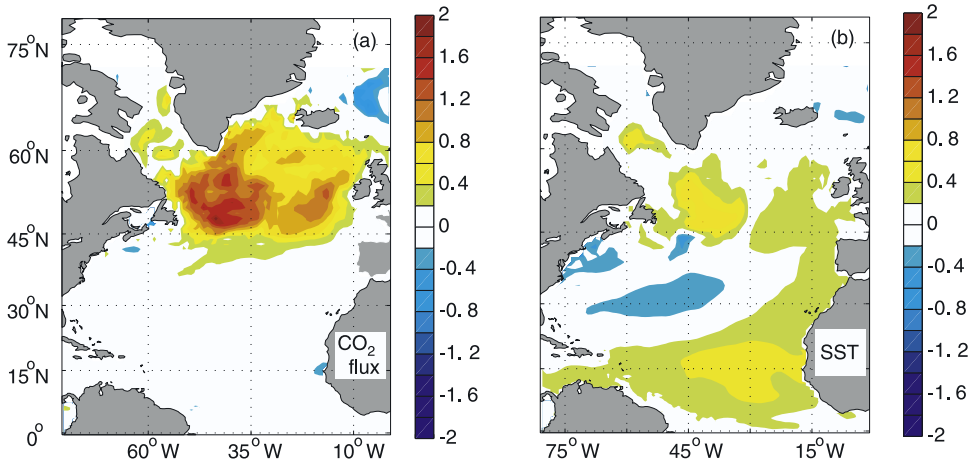

Figure 8. (a) First EOF of air-sea flux of CO_2 (mol m^{-2} yr^{-1}) and (b) first EOF of SST (°C) in the North Atlantic (15°N–80°N). EOF1 of air-sea CO_2 flux explains 11% of the variance; EOF1 of SST explains 15% of the variance. Both EOFs are based on monthly data.

export flux captures 17% of the interannual variance with PC1 correlating with the NAO at r = 0.60 (not shown).

[34] In the model's subpolar gyre, surface DIC variability is primarily controlled by convection (Figure 10a). Export production, responding to the concurrent changes in nutrient supply, counters the convective DIC supply with strong carbon export, and some variability in storage, $\frac{dDIC}{dt}$, results. Yet the air-sea flux resulting from convective DIC anomalies is small and decoupled from the physical forcing. In contrast, in the same model, O_2 air-sea flux variability is significant in the subpolar North Atlantic (Figure 10b) and tightly related to the convective mixing. Why do these gases behave so differently in the North Atlantic?

[35] First, consider the seasonal cycles of CO_2 and O_2 and their relationship to vertical transport (convection and export production) and temperature anomalies. When summer warming occurs, biological production also occurs, and both processes drive an efflux of O_2 from the surface. In winter, convective mixing occurs and brings low O_2 waters to the surface, and also cooling reduces surface pO_2, both driving an influx of O_2 from the atmosphere. In contrast, warm summer surface waters promote high pCO_2 whereas biological production reduces pCO_2, and winter convection exposes high pCO_2 to the surface while cooling reduces pCO_2. Through this mechanism, there is a damping of surface pCO_2 anomalies and an enhancement of O_2 flux anomalies. This model indicates a similar relationship to be partly responsible for the difference in North Atlantic gas flux variability for CO_2 and O_2 on interannual timescales. Temperature and DIC-driven pCO_2 anomalies tend to be anti-correlated across the North Atlantic, with temperature dominating in the subtropics and DIC dominating in the subpolar gyres (Figure 9). *McKinley et al.* [2003] show that interannual variability in heat fluxes and air-sea O_2 fluxes are positively correlated across the North Atlantic. However, this mechanism is not the primary reason for the large difference in the magnitude of the modeled CO_2 and O_2 flux anomalies in the North Atlantic.

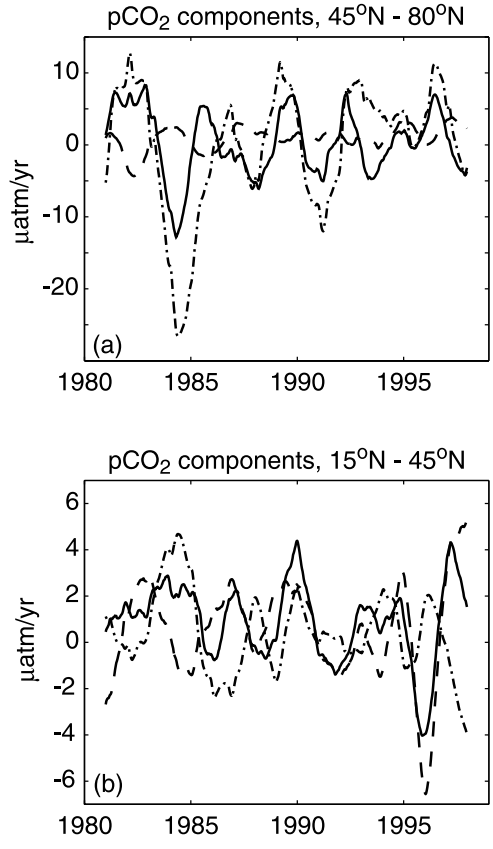

Figure 9. Components of pCO_2 (µatm yr^{-1}) interannual variabilty in (a) subpolar North Atlantic (45°N–80°N) and (b) subtropical North Atlantic (15°N–45°N), showing $\frac{dpCO_2}{dt}$ (thin solid line), $\frac{\delta pCO_2}{\delta T}\frac{dT}{dt}$ (dashed line), and $\frac{\delta pCO_2}{\delta DIC}\frac{dDIC}{dt}$ (dash-dotted line). Each term is calculated from modeled variability in the forcing of interest (e.g., DIC, T, ALK, S) while other forcings are held constant. Variability in $\frac{\delta pCO_2}{\delta ALK}\frac{dALK}{dt}$ and $\frac{\delta pCO_2}{\delta S}\frac{dS}{dt}$ are small and are not shown. For clarity, time series are twice smoothed over 12 months.

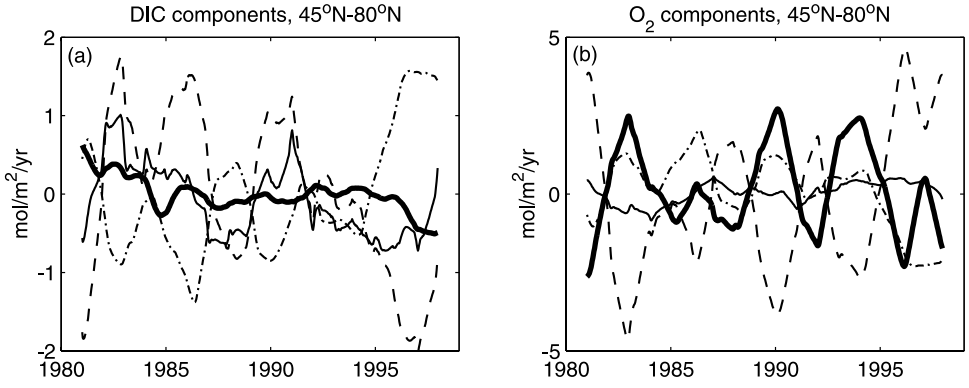

Figure 10. Components of (a) DIC and (b) O_2 interannual variability in the subpolar North Atlantic (45°N–80°N) in mol m^{-2} yr^{-1}: $\frac{dDIC}{dt}$, $\frac{dO_2}{dt}$ (thin solid line), convection (dashed line), export production (dash-dotted line), and air-sea flux (bold solid line). Advection and freshwater terms have little influence on the total variability and are not shown. For clarity, time series are twice smoothed over 12 months.

[36] Our model indicates that CO_2 flux anomalies are smaller than those of O_2 primarily because CO_2 has a much longer air-sea equilibration timescale. This creates a very different balance in the surface response to DIC anomalies than for O_2 anomalies. Owing to carbonate chemistry, the equilibration time for CO_2 is approximately 20 times longer than for O_2, which does not react with seawater. Depending on the mixed layer thickness and other factors, O_2 equilibrates within a few weeks and CO_2 may take a year or more [*Broecker and Peng*, 1974]. Much of the variability in the North Atlantic is driven by interannual changes in convective mixing which is acting on short timescales (a few weeks) primarily at the end of each winter. Following deep winter convection, rapid springtime biological drawdown and export neutralizes much of the convectively driven DIC anomaly before air-sea exchange can have a significant impact (Figure 10a). The O_2 equilibration response via air-sea exchange, however, occurs on a timescale comparable to, or faster than, the biological drawdown. Rapid equilibration of O_2 anomalies by the air-sea flux means that there is little temporal change in the surface O_2 inventory ($\frac{dO_2}{dt}$). Thus CO_2 and O_2 fluxes exhibit very different responses to convectively driven anomalies in the subpolar Atlantic. The dominant oxygen balance is between anomalies in vertical transport (convection and biological export) and air-sea exchange; but for DIC, the balance is primarily between the two vertical transport terms.

[37] The slow equilibration of CO_2 through gas exchange is also important to decoupling the CO_2 flux response in the model's subtropical gyre. The temperature term of equation (3) has a small correlation with the NAO (r = 0.37) in the subtropics, indicating that the forcing of pCO_2 anomalies is related to the NAO index via the influence of SST [*Gruber et al.*, 2002]. However, due to the slow equilibration timescale for CO_2, the air-sea flux resulting from these anomalies has little relationship to the NAO. Lateral advection and other forcings act rapidly to disperse and eliminate anomalies before such a relationship can be established locally. This is in strong contrast to the oxygen fluxes which showed a clear relationship to the physical forcing and NAO index in the subtropics [*McKinley et al.*, 2003].

[38] Our model suggests a decoupling of the air-sea carbon flux from the physical forcing, NAO index, and oxygen fluxes in the North Atlantic which is attributable to the long air-sea equilibration timescale for CO_2, and also to anti-correlation of temperature and vertical transport (convection and export production) influences on pCO_2 variability. Thus it may not possible to extrapolate observed flux variability at Bermuda over the basin as suggested by *Gruber et al.* [2002]. We illustrate this in Figure 11 by mapping the correlation of the modeled air-sea CO_2 flux variability at Bermuda with each model grid point in the North Atlantic. There is a correlation of the flux variability across a large region of the subtropical gyre which has a weak association with the NAO. However, Figure 11 clearly

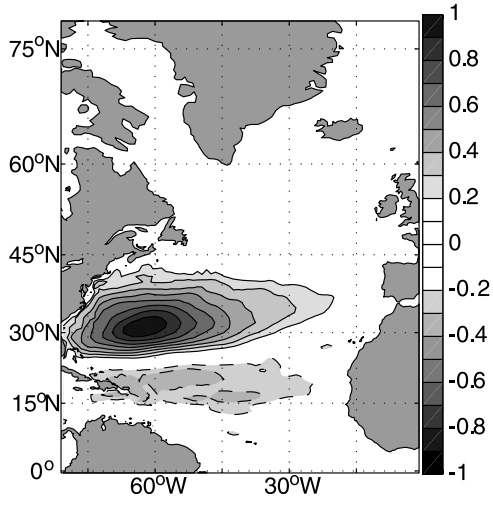

Figure 11. Point correlation between modeled air-sea CO_2 flux variability at Bermuda and at each point in the North Atlantic. Negative values are indicated by the dashed lines.

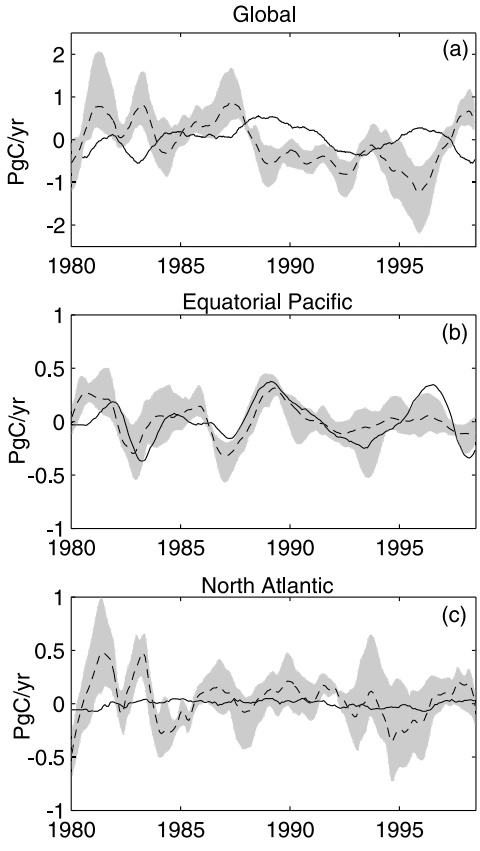

Figure 12. Comparison of our modeled (solid line) integrated air-sea CO_2 flux anomalies and those from the atmospheric inversion of *Bousquet et al.* [2000] (dashed lines with gray bands that are the range from seven inversions) for (a) the global air-sea flux variability, (b) the equatorial Pacific, and (c) the North Atlantic, in PgC yr^{-1}. Detrended model anomalies about the 1980–1998 time mean are shown.

illustrates that there is no correlation of the flux variability in the subpolar gyre or even over a large fraction of the subtropics.

4.3. Implications for Atmospheric Inversions

[39] How does the interannual variability of the air-sea flux of CO_2 estimated by this model compare with atmospheric inverse models, such as that of *Bousquet et al.* [2000]? In Figure 12a we compare time series of the global air-sea flux anomalies from the two approaches. Although the magnitude of the flux variability is similar between the two methods, the temporal structures are entirely different. There is very good agreement between the methods in the equatorial Pacific region (Figure 12b), but in the North Atlantic (Figure 12c) the atmospheric inversion suggests much more variability than implied by the ocean model. In fact, *Bousquet et al.* [2000] find significantly greater air-sea flux variability in all high-latitude regions than in the ocean model (Peylin et al., submitted manuscript, 2004). In the inversion, the temporal structure of the global time series is dominated by the high latitudes, while our ocean model, consistent with the studies of *Obata and Kitamura* [2003], *LeQuéré et al.* [2000] and *Winguth et al.* [1994], indicates that the equatorial Pacific dominates the global budget (Figure 5).

[40] We note that if the range of the seven inversions performed by *Bousquet et al.* [2000] is taken as an uncertainty, our ocean model result is only distinguishable from the inversion in the North Atlantic for a few short periods of time (Figure 12c), particularly after 1985, when the inversion benefits from more data and is considered by the authors to be more reliable (Peylin et al., submitted manuscript, 2004). Thus it is possible that the uncertainty in the inversion (and, of course, in the ocean model) may be simply too large for conclusions to be drawn. However, for the sake of this discussion, we will assume that the mean of the seven inversion runs provides evidence for an appreciable difference from the ocean models.

[41] Why might it be that there is such a difference between estimates of air-sea CO_2 flux variability from the two methods in the North Atlantic, while at the same time agreement is extremely good in the equatorial Pacific? Damped physical variability in the ocean models is likely part of the answer (Peylin et al., submitted manuscript, 2004). Indeed, our model does under-represent sea surface height variability [*McKinley*, 2002] and captures much, but not all, of the mixed layer depth variability at Bermuda and Hawaii (Figure 1). However, SST variability comparisons (Figure 2) indicate that the degree of physical variability captured by the model is no different at high latitudes than in the tropics. The model also captures much of the observed air-sea CO_2 flux variability at Bermuda and Hawaii (Figure 4), indicating good subtropical performance. An additional factor might be the highly idealized parameterization of biological processes in the ocean model, which could lead to unrealistic balances and fluxes. However, the recent study of *LeQuéré et al.* [2003] does not support this explanation.

[42] In addition, assumptions in the atmospheric inversions may also lead to errors in the flux estimates. Atmospheric inversions have difficulty discriminating between land and ocean regions at similar latitudes due to rapid zonal mixing in the atmosphere. Further, we postulate that they may be biased to overestimate high-latitude air-sea flux variability by assuming that variability in CO_2 fluxes is driven by modulation of the amplitude of monthly mean fluxes [*Takahashi et al.*, 1997] across large regions of the ocean. Our ocean model indicates that while this assumption may be appropriate in the equatorial Pacific, it is not applicable to the North Atlantic (or other extratropical regions). We find that a very large portion (50%) of the CO_2 flux variability in the equatorial Pacific between 15°S and 15°N is associated with a pattern (EOF1) that reflects both the mean air-sea flux and monthly flux patterns. ENSO drives physical changes across the whole of the equatorial Pacific, and does so on timescales long enough for a significant air-sea flux anomaly to occur. In contrast, variability in the North Atlantic does not occur with significant basin-scale coherence: EOF1 captures only 11% of the interannual variability in this region (Figure 8a). The

spatial pattern of the flux variability is dominated by brief, small-scale convective anomalies that have little coherence from year to year. The potential flux variability driven by these anomalies is damped primarily by export production that occurs on timescales faster than the air-sea exchange of CO_2 (Figure 10a).

[43] *Kaminski et al.* [2001] show that the aggregation of fluxes from the resolution of a transport model to fixed patterns over large spatial areas can cause significant errors in atmospheric inversions for the seasonal cycle of CO_2 sources and sinks. They show these "aggregation errors" to be of comparable magnitude to the fluxes of interest. In some cases, spatially non-uniform a priori estimates can increase aggregation errors, while in other cases the non-uniform a priori basis function can significantly reduce the aggregation error. With models and observation, we have shown that the a priori spatial pattern used to calculate the basis functions in the work of *Bousquet et al.* [2000] in the equatorial Pacific is likely to be a reasonable representation of the true flux variability pattern, and thus it is likely to improve the inversion. At the same time, our model suggests that the a priori patterns used in the North Atlantic may not be consistent with the true variability, and thus aggregation errors may be aggravated in this region.

[44] If sufficient atmospheric data were available, the use of smaller regions in the high latitudes might lead to smaller estimates of high-latitude CO_2 flux variability in the inversions and increased agreement between the ocean models and the atmospheric inversions [*Kaminski et al.*, 2001; *Rodenbeck et al.*, 2003]. Additionally, now that ocean model estimates of CO_2 flux variability are able to capture a great deal of the observed local CO_2 flux variability (Figure 4), it is possible that interannual CO_2 flux inversions may be improved by projecting onto patterns of CO_2 flux variability from an ocean model (with appropriate uncertainties), instead of the climatological flux patterns.

5. Conclusions

[45] For the period 1980-1998, our ocean model suggests peak-to-peak global air-sea CO_2 flux variability of ±0.5 PgC yr^{-1} (RMS = 0.28 PgC yr^{-1}). Physical variability in the equatorial Pacific associated with ENSO is the primary driver of global air-sea CO_2 flux variability. Changes in the slope of the thermocline across the equatorial Pacific, in the efficiency of upwelling, and in the longitudinal displacement of the western Pacific warm pool significantly alter the supply of DIC to the surface over a large ocean area. The resulting pCO_2 variability combines with ENSO-related wind speed variations, and a substantial air-sea flux variability results. In the North Atlantic, air-sea CO_2 flux variability is small. Biogenic export counters flux tendencies created by variability in convection driven in part by the NAO. Slow CO_2 equilibration via gas exchange allows the seasonal and interannual CO_2 flux balance to be between convection and export, which results in little CO_2 air-sea flux variability from this region. This is in strong contrast to the balances for O_2 which has a much shorter air-sea equilibration timescale. Furthermore, our model indicates that while flux variability at Bermuda may provide some information about a substantial portion of the subtropical gyre, it is not a good predictor of basin-scale air-sea CO_2 flux variability.

[46] Ocean model estimates of air-sea CO_2 flux variability compare well to the atmospheric inversion of *Bousquet et al.* [2000] in the equatorial Pacific, but do not agree with the inversion result in the North Atlantic. Drawing on the model's illustration of substantial large-scale spatial coherence of the flux variability in the equatorial Pacific and a lack of coherence in the North Atlantic, we speculate that a priori assumptions about the geographic patterns of the flux variability may be responsible for biasing the atmospheric inversions toward over-representation of high-latitude air-sea CO_2 flux variability.

[47] In order to improve our knowledge of the mechanisms discussed here, the impact of ocean physical variability on biogeochemical variability must be better understood. This requires better models and also substantially more data. High-latitude ocean time series stations, particularly in the subpolar North Atlantic, and an increased network for measurements of atmospheric CO_2 and other gases are key to our improved understanding of global and regional air-sea CO_2 flux variability.

[48] **Acknowledgments.** We thank the JPL ECCO group for MITgcm output; C. Hill and S. Dutkiewicz for modeling assistance; and N. Gruber, H. Brix, P. Bousquet, and P. Peylin for making data and results available. We also thank R. Wanninkhof, N. Gruber, and an anonymous reviewer for their helpful comments. Local cluster computational resources were made available by Digital Equipment, Intel Corporation, and Sun Microsystems. G. A. M. thanks NASA for the Earth System Science Fellowship (NGT5-30189). M. J. F. is grateful for support from NOPP (grant N00014-02-1-0370) and NOAA (NA16GP2988).

References

Anderson, L. A., and J. L. Sarmiento (1994), Redfield ratios of remineralization determined by nutrient data analysis, *Global Biogeochem. Cycles*, *8*, 65–80.

Bates, N. R. (2001), Interannual variability of oceanic CO_2 and biogeochemical properties in the western North Atlantic subtropical gyre, *Deep Sea Res., Part II*, *48*, 1507–1528.

Bender, M., T. Ellis, P. P. Tans, R. Francey, and D. Lowe (1996), Variability in the O_2/N_2 ratio of the Southern Hemisphere air, 1991–1994: Implications for the carbon cycle, *Global Biogeochem. Cycles*, *10*, 9–21.

Bousquet, P., P. Peylin, P. Ciais, C. LeQuéré, P. Friedlingstein, and P. Tans (2000), Regional changes in carbon dioxide fluxes of land and oceans since 1980, *Science*, *290*, 1342–1346.

Boutin, J., et al. (1999), Satellite sea surface temperature: A powerful tool for interpreting in situ pCO_2 measurements in the equatorial Pacific Ocean, *Tellus, Ser. B*, *51*, 490–508.

Broecker, W. S., and T. H. Peng (1974), Gas exchange rates between air and sea, *Tellus*, *26*, 21–34.

Campbell, J. A. (1983), The geochemical oceans sections study—GEOSECS, in *Chemical Oceanography*, vol. 8, edited by J. P. Riley and R. Chester, pp. 89–155, Academic, San Diego, Calif.

Chavez, F. P., P. G. Strutton, G. E. Friederich, R. A. Feely, G. C. Feldman, D. G. Foley, and M. J. McPhaden (1999), Biological and chemical response of the equatorial Pacific Ocean to the 1997–98 El Niño, *Science*, *286*, 2126–2131.

Conkright, M., et al. (1998), World Ocean Atlas 1998: Data Set Documentation [CD-ROM], *Tech. Rep. 15*, Natl. Oceanic and Atmos. Admin., Silver Spring, Md.

Conway, T. J., P. P. Tans, L. S. Watermann, K. W. Thoning, D. R. Kitzis, K. A. Masarie, and N. Zhang (1994), Evidence for interannual variability of the carbon cycle from the National Oceanic and Atmospheric Administration/Climate Monitoring and Diagnostics Laboratory Global Air Sampling Network, *J. Geophys. Res.*, *99*(D11), 22,831–22,855.

Cosca, C. E., R. A. Feely, J. Boutin, J. Etcheto, M. J. McPhaden, F. P. Chavez, and P. G. Strutton (2003), Seasonal and interannual CO_2 fluxes for the central and eastern equatorial Pacific Ocean as determined from

fCO_2-SST relationships, *J. Geophys. Res.*, *10*(C8), 3278, doi:10.1029/2000JC000677.

da Silva, A., A. C. Young, and S. Levitus (1994), Atlas of Surface Marine Data, *NOAA Atlas NESDIS 6*, 83 pp., Natl. Oceanic and Atmos. Admin., Silver Spring, Md.

Dickson, R., J. Lazier, J. Meinke, P. Rhines, and J. Swift (1996), Long-term co-ordinated changes in the convective activity of the North Atlantic, *Prog. Oceanogr.*, *38*, 241–295.

Dore, J. E., R. Lukas, D. W. Sadler, and D. M. Karl (2003), Climate-driven changes to the atmospheric CO_2 sink in the subtropical North Pacific Ocean, *Nature*, *424*, 754–757.

Dutay, J.-C., et al. (2002), Evaluation of ocean model ventilation with CFC-11: Comparison of 13 global ocean models, *Ocean Modell.*, *4*, 89–120.

Dutkiewicz, S., M. Follows, J. Marshall, and W. W. Gregg (2001), Interannual variability of phytoplankton abundances in the North Atlantic, *Deep Sea Res., Part II*, *48*, 2323–2344.

Feely, R. A., R. Wanninkhof, T. Takahashi, and P. Tans (1999), Influence of El Niño on the equatorial Pacific contribution to atmospheric CO_2 accumulation, *Nature*, *398*, 365–386.

Feely, R. A., et al. (2002), Seasonal and interannual variability of CO_2 in the equatorial Pacific, *Deep Sea Res., Part II*, *49*, 2443–2469.

Follows, M. J., R. G. Williams, and J. C. Marshall (1996), The solubility pump of carbon in the subtropical gyre of the North Atlantic, *J. Mar. Res.*, *54*, 605–630.

Francey, R. J., C. E. Allison, C. M. Trudinger, P. J. Rayner, I. G. Enting, and L. P. Steele (2001), The interannual variation in global atmospheric $\delta^{13}C$ and its link to net terrestrial exchange, paper presented at 6th International Carbon Dioxide Conference, Grad. School of Sci., Tohoku Univ., Sendai, Japan.

Gent, P. R., and J. C. McWilliams (1990), Isopycnal mixing in ocean general circulation models, *J. Phys. Oceanogr.*, *20*, 150–155.

Goyet, C., R. Healy, and J. Ryan (2000), Global distribution of total inorganic carbon and total alkalinity below the deepest winter mixed layer depths, *Tech. Rep. NDP-076*, Carbon Dioxide Inf. Anal. Cent., Oak Ridge, Tenn.

Gruber, N., C. D. Keeling, and N. R. Bates (2002), Interannual variability in the North Atlantic Ocean carbon sink, *Science*, *298*, 2374–2378.

Gurney, K., et al. (2002), Towards robust regional estimates of CO_2 sources and sinks using atmospheric transport models, *Nature*, *415*, 626–630.

Hurrell, J. W. (1995), Decadal trends in the North Atlantic Oscillation: Regional temperatures and precipitation, *Science*, *269*, 676–679.

Kalnay, E., et al. (1996), The NCEP/NCAR 40-Year Reanalysis Project, *Bull. Am. Meteorol. Soc.*, *77*, 437–471.

Kaminski, T., P. J. Rayner, M. Heimann, and I. G. Enting (2001), On aggregation errors in atmospheric transport inversions, *J. Geophys. Res.*, *106*(D5), 4703–4715.

Karl, D. M., and R. Lukas (1996), The Hawaii Ocean Time-series (HOT) program: Background, rationale and field implementation, *Deep Sea Res., Part II*, *43*, 129–156.

Keeling, C. D., and T. P. Whorf (2000), Atmospheric CO_2 Concentrations—Mauna Loa Observatory, Hawaii, 1958–1999 (revised August 2000), *Tech. Rep. NDP-001*, Carbon Dioxide Inf. Anal. Cent., Oak Ridge, Tenn.

Keeling, R. F., S. C. Piper, and M. Heimann (1996), Global and hemispheric CO_2 sinks deduced from changes in atmospheric O_2 concentration, *Nature*, *381*, 150–155.

Large, W. G., J. C. McWilliams, and S. C. Doney (1994), Oceanic vertical mixing: A review and a model with a nonlocal boundary layer parameterization, *Rev. Geophys.*, *32*, 363–403.

Lee, T., I. Fukimori, D. Menemenlis, Z. Xing, and L. L. Fu (2002), Effects of Indonesian throughflow on the Pacific and Indian Ocean, *J. Phys. Oceanogr.*, *32*, 1404–1429.

Le Quéré, C., J. C. Orr, P. Monfray, O. Aumont, and G. Madec (2000), Interannual variability of the oceanic sink of CO_2 from 1979 to 1997, *Global Biogeochem. Cycles*, *14*, 1247–1265.

LeQuéré, C., O. Aumont, P. Monfray, and J. C. Orr (2003), Propagation of climatic events on ocean stratification, marine biology, and CO_2: Case studies over the 1979–1999 period, *J. Geophys. Res.*, *108*(C12), 3375, doi:10.1029/2001JC000920.

Maier-Reimer, E. (1993), Geochemical cycles in an ocean general circulation model: Preindustrial tracer distributions, *Global Biogeochem. Cycles*, *7*, 645–677.

Manning, A. C. (2001), Temporal variability of atmospheric oxygen from both continuous measurements and a flask sampling network: Tools for studying the global carbon cycle, Ph.D. thesis, Univ. of Calif., San Diego.

Marshall, J., and F. Molteni (1993), Toward a dynamical understanding of planetary-scale flow regimes, *J. Atmos. Sci.*, *50*, 1792–1818.

Marshall, J. C., C. Hill, L. Perelman, and A. Adcroft (1997a), Hydrostatic, quasi-hydrostatic and non-hydrostatic ocean modeling, *J. Geophys. Res.*, *102*, 5733–5752.

Marshall, J. C., A. Adcroft, C. Hill, L. Perelman, and C. Heisey (1997b), A finite volume, incompressible Navier-Stokes model for studies of the ocean on parallel computers, *J. Geophys. Res.*, *102*, 5753–5766.

Martin, J., et al. (1994), Testing the iron hypothesis in ecosystems of the equatorial Pacific Ocean, *Nature*, *371*, 123–129.

McKinley, G. A. (2002), Interannual variability of air-sea fluxes of carbon dioxide and oxygen, Ph.D. thesis, Mass. Inst. of Technol., Cambridge.

McKinley, G. A., M. J. Follows, and J. Marshall (2000), Interannual variability of the air-sea flux of oxygen in the North Atlantic, *Geophys. Res. Lett.*, *27*, 2933–2936.

McKinley, G. A., M. J. Follows, J. Marshall, and S. Fan (2003), Interannual variability in air-sea O_2 fluxs and the determination of CO_2 sinks using atmospheric O_2/N_2, *Geophys. Res. Lett.*, *30*(3), 1101, doi:10.1029/2002GL016044.

McPhaden, M. J., et al. (1998), The Tropical Ocean-Global Atmosphere observing system: A decade of progress, *J. Geophys. Res.*, *103*(C7), 14,169–14,2400.

Monterey, G., and S. Levitus (1997), *Seasonal Variability of Mixed Layer Depth for the World Ocean*, *NOAA Atlas, NESDIS 14*, 100 pp., Natl. Oceanic and Atmos. Admin., Silver Spring, Md.

Obata, A., and Y. Kitamura (2003), Interannual variability of the sea-air exchange of CO_2 from 1961 to 1998 simulated with a global ocean circulation-biogeochemisty model, *J. Geophys. Res.*, *108*(C11), 3337, doi:10.1029/2001JC001088.

Rayner, P. J., I. G. Enting, R. J. Francey, and R. Langenfelds (1999a), Reconstructing the recent carbon cycle from atmospheric CO_2, $\delta^{13}C$ and O_2/N_2 observations, *Tellus, Ser. B*, *51*, 213–232.

Rayner, P. J., R. Law, and R. Dargaville (1999b), The relationship between tropical CO_2 fluxes and the El Niño-Southern Oscillation, *Geophys. Res. Lett.*, *26*, 493–496.

Reynolds, R. W., and T. M. Smith (1994), Improved global sea surface temperature analyses, *J. Clim.*, *7*, 929–948.

Rodenbeck, C., S. Houweling, M. Gloor, and M. Heimann (2003), CO_2 flux history 1982–2001 inferred from atmospheric data using a global inversion of atmospheric transport, *Atmos. Chem. Phys.*, *3*, 1919–1964.

Stammer, D., R. Tokmakian, A. Semtner, and C. Wunsch (1996), How well does a 1/4° global circulation model simulate large-scale oceanic observations?, *J. Geophys. Res.*, *101*(C10), 25,779–25,811.

Takahashi, T., W. S. Broecker, and A. E. Brainbridge (1981), The alkalinity and total carbon dioxide concentrations in the world oceans, *Carbon Cycle Modell.*, edited by B. Bolin, John Wiley, New York.

Takahashi, T., J. Olafsson, J. G. Goddard, D. W. Chipman, and S. C. Sutherland (1993), Seasonal variation of CO_2 and nutrients in the high-latitude surface oceans: A comparative study, *Global Biogeochem. Cycles*, *7*, 843–878.

Takahashi, T., R. A. Feely, R. F. Weiss, R. H. Wanninkhof, D. W. Chipman, S. C. Sutherland, and T. Takahashi (1997), Global air-sea flux of CO_2: An estimate based on measurements of sea-air pCO_2 difference, *Proc. Natl. Acad. Sci. USA*, *94*, 8292–8299.

Takahashi, T., et al. (2002), Global sea-air CO_2 flux based on climatological surface ocean pCO_2, and seasonal biological and temperature effects, *Deep Sea Res., Part II*, *49*, 1601–1622.

Wanninkhof, R. (1992), Relationship between wind speed and gas exchange over the ocean, *J. Geophys. Res.*, *97*, 7373–7382.

Williams, R. G., and M. J. Follows (1998), The Ekman transfer of nutrients and maintenance of new production over the North Atlantic, *Deep Sea Res., Part I*, *45*, 461–489.

Williams, R. G., A. J. McLaren, and M. J. Follows (2000), Estimating the convective supply of nitrate and implied variability in export production over the North Atlantic, *Global Biogeochem. Cycles*, *14*, 1299–1313.

Winguth, A. M. E., M. Heimann, K. D. Kurz, E. Maier-Reimer, U. Milolajewicz, and J. Segschneider (1994), El Niño-Southern Oscillation related fluctuations in the marine carbon cycle, *Global Biogeochem. Cycles*, *8*, 39–93.

M. J. Follows and J. Marshall, Department of Earth, Atmospheric and Planetary Sciences, Massachusetts Institute of Technology, 77 Massachusetts Avenue, Cambridge, MA 02139, USA.

G. A. McKinley, Department of Atmospheric and Oceanic Sciences, University of Wisconsin-Madison, 1225 West Dayton Street, Madison, WI 53706, USA. (galen@aos.wisc.edu)